Chapter 5

Conductive Hybrid Hydrogel of Carbon Nanotubes-Protein-Cellulose: In vivo Treatment of Diabetic Wound via Photothermal Therapy and Tracking Real-Time Wound Assessment via Photoacoustic Imaging

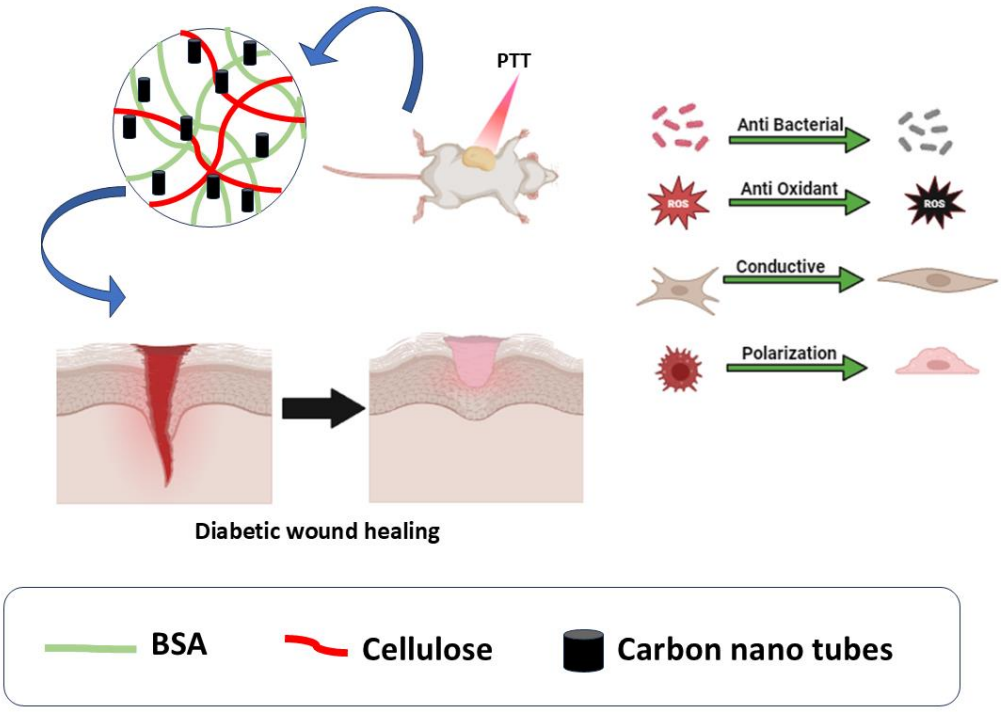

Schematic 3: Performance of B+C+CNT hydrogel for accelerated diabetic wound healing by NIR stimulation

5.1 Introduction

Diabetes mellitus (DM) is a rapidly growing global health concern, with a significant number of patients suffering from diabetic foot ulcers (DFUs), one of its most severe complications[143]. Chronic wounds such as DFUs are particularly challenging to heal, leading to infections, prolonged hospitalizations, and in severe cases, amputations[144][145]. The impaired wound healing in diabetes arises due to factors like impaired angiogenesis, neuropathy, chronic inflammation, and reduced oxygenation[145]. Conventional treatments often struggle to address the underlying issues, necessitating the development of innovative wound care strategies that can actively promote tissue regeneration and tackle complications associated with diabetic wounds[145][146]. In recent years, hydrogels have emerged as promising candidates for wound healing due to their ability to provide a moist environment, protect against infections, and support cellular activities[41][147]. Hydrogels can be designed to deliver drugs, growth factors, and even stem cells, enhancing the wound healing process. However, traditional hydrogels have limitations, such as poor mechanical strength and an inability to actively participate in biological processes like cellular communication[148]. These shortcomings have led to the exploration of advanced materials, including conductive hydrogels, which offer an exciting avenue for more effective diabetic wound healing solutions[149].

Conductive hydrogels have gained attention due to their ability to mimic the electrical properties of natural tissues[150][151]. The electrical signals in biological systems are known to regulate various cellular processes, including proliferation, migration, and differentiation, all of which are crucial for tissue repair[152]. By incorporating conductive elements into the

hydrogel matrix, these materials can enhance cellular communication and promote faster wound healing[153]. Carbon nanotubes (CNTs), with their excellent electrical, thermal, and mechanical properties, have become a leading choice for enhancing the conductivity of hydrogels[154][155]. CNTs can facilitate electron transport, improving the hydrogel's ability to communicate electrical signals to cells, which plays a vital role in tissue regeneration[156]. Moreover, CNTs exhibit photothermal properties, which can be utilized to further enhance the therapeutic potential of hydrogels. When exposed to near-infrared (NIR) light, CNTs absorb the energy and convert it into localized heat, creating a photothermal effect[157]. This heating can aid in several aspects of wound healing, such as increasing blood flow to the wound site, accelerating tissue metabolism, and even reducing bacterial load through thermal inactivation[158]. The combination of conductivity and photothermal properties makes CNTs highly versatile for designing multifunctional hydrogels tailored for complex wounds like DFUs.

One of the key challenges in wound healing research is the ability to monitor the progression of healing in real-time[159]. Traditional methods, such as histological analysis, only provide snapshots of the wound at specific time points and are invasive. Photoacoustic imaging (PAI), an emerging non-invasive imaging technique, offers a novel solution[33]. PAI combines the advantages of optical and ultrasound imaging, allowing for deep tissue imaging with high spatial resolution. It is particularly useful for monitoring blood oxygenation and vascularization, critical parameters in the wound healing process[34].

In this study, we present the development and in vivo application of a novel carbon nanotube-based conductive protein-cellulose hydrogel for the treatment of diabetic wounds as depicted in schematic 3. Bovine serum albumin (BSA), as a protein, enhances biocompatibility and

mimics native extracellular matrix properties, facilitating cell adhesion and proliferation essential for tissue repair[160][161]. Its presence also introduces amino groups that can participate in cross-linking, contributing to the hydrogel's stability and controlled degradation, which is beneficial for sustained therapeutic action at the wound site[162]. Cellulose, as a natural polysaccharide, imparts robust structural integrity while providing a porous network conducive to nutrient and oxygen exchange, which is critical for cell viability in the wound environment[163]. Furthermore, cellulose's inherent hydrophilicity aids in moisture retention, creating an optimal wound-healing environment by preventing excessive dryness. Combined, BSA and cellulose create a synergistic framework that supports cellular functions and ensures mechanical durability, which is particularly advantageous in diabetic wound care, where prolonged healing time The hydrogel leverages the electrical conductivity of CNTs to promote cellular activities essential for tissue repair and utilizes the photothermal properties of CNTs to enhance the wound healing process. By applying NIR irradiation, we hypothesize that the dual action of electrical stimulation and localized heating will result in accelerated wound closure, reduced inflammation, and improved tissue regeneration. Additionally, we employ photoacoustic imaging to non-invasively monitor the wound healing process, focusing on changes in vascularization and oxygenation over time. This approach is, to the best of our knowledge, the first of its kind to combine CNTs with a protein-cellulose hydrogel matrix for diabetic wound healing. Our goal is to demonstrate that this multifunctional hydrogel not only enhances the rate of wound healing but also provides a platform for non-invasive, real-time monitoring of the healing process. Additionally, we also evaluated pharmacological properties of hydrogels on diabetic wounds by histopathology and immunohistochemistry. The findings of this study have the potential to advance the field of

wound care, offering new therapeutic strategies for managing chronic wounds in diabetic patients.

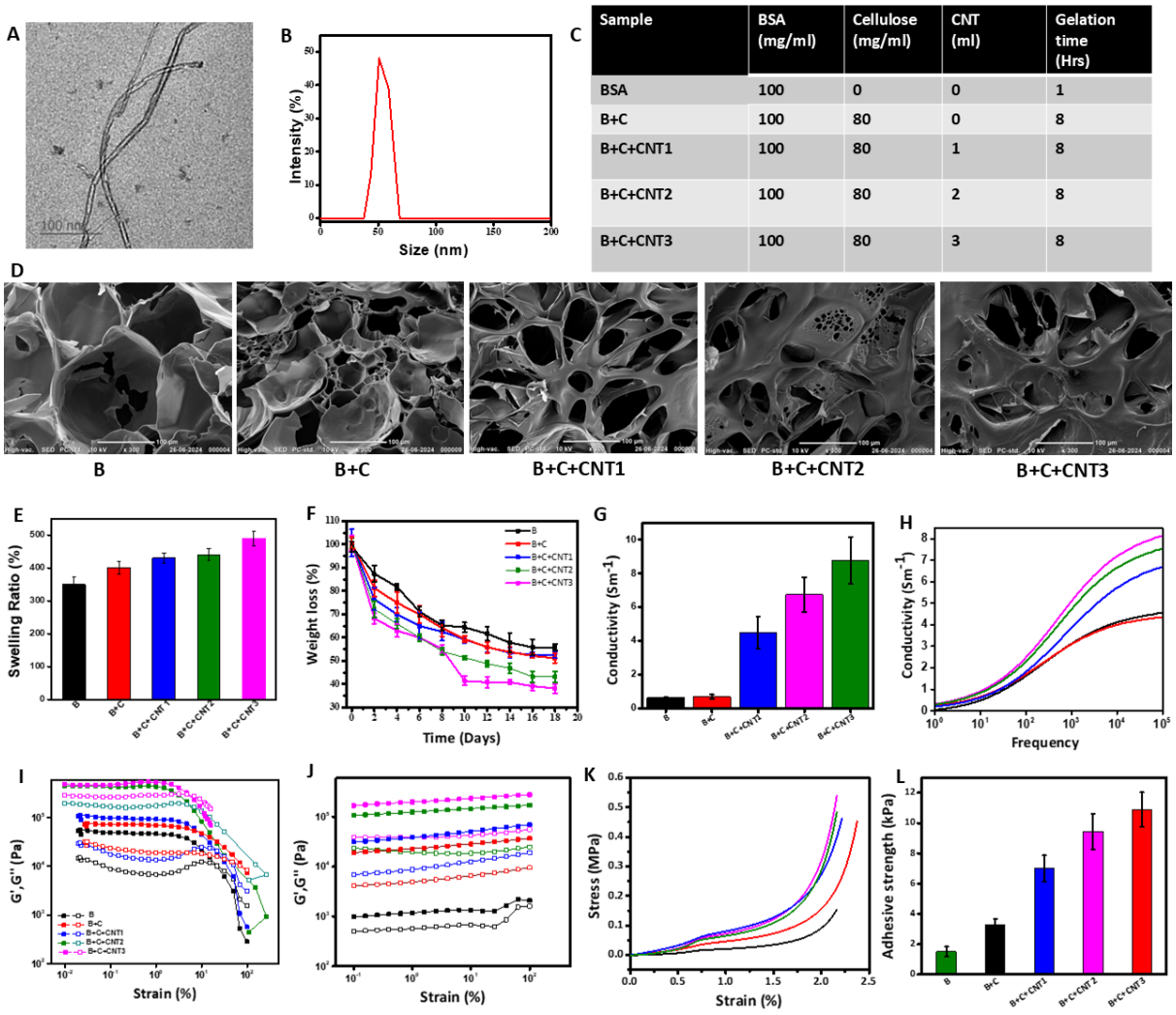

Sample	BSA (mg/ml)	Cellulose (mg/ml)	CNT (ml)	Gelation time (Hrs)
BSA	100	0	0	1
B+C	100	80	0	8
B+C+CNT1	100	80	1	8
B+C+CNT2	100	80	2	8
B+C+CNT3	100	80	3	8

Figure 5.1 Physiochemical Characterizations (A) TEM image of CNTs (B) DLS of CNTs (C) Composition BSA, Cellulose and CNTs in hydrogels (D) SEM images of composite hydrogels (E) Equilibrium Swelling ratio after 24 hrs (F) Weight loss degradation study of hydrogels over 18 days (G) two probe Conductivity of B+C+CNT hydrogels (H) EIS measurement of conductivity Rheological characterization: (I) Amplitude Sweep at constant frequency 10 rad/s to determine LVER (J) Frequency sweep at constant strain (K) Compression test (L) Adhesion test (Dats is represented as Mean± SEM (n=3))

5.2 Results and discussion

5.2.1 Characterization of CNT

Characterization of CNTs was carried out using Transmission Electron Microscopy (TEM) and Dynamic Light Scattering (DLS). TEM imaging (Fig 5.1A) revealed a clear visualization of the CNT structure with a diameter size around 20 nm, providing precise insights into the physical dimensions of individual nanotubes. This fine scale of 20 nm as observed by TEM allows for understanding of the inherent nanoscale features critical for biomedical applications, including surface morphology and tube diameter, which influence cell interaction and conductive properties. Also, when analysing the CNTs in an aqueous environment using DLS, a different size profile was observed (Fig 5.1B), with an average hydrodynamic size around 40 nm. This increase in apparent size with DLS is likely due to the hydration shell and possible aggregation that occurs in the suspension medium, resulting in a larger overall particle size measurement.

5.2.2 Formation of hydrogels

The hybrid hydrogels were synthesized by heating precursor solutions above the melting temperature of BSA. The compositions of the hydrogels are provided in Fig 5.1C. This process resulted in the formation of a translucent gel that passed the vial inversion test within a short period. All preheated solutions exhibited a significantly high negative zeta potential. These zeta potential values reflect a substantial presence of surface charges on the protein, which promotes excellent dispersion stability and prevents BSA aggregation through electrostatic repulsion. The heat-induced gelation of BSA is a well-documented

phenomenon[68]. At elevated temperatures and pH levels far from BSA's isoelectric point (~4. 5) aggregation is initiated by the partial unfolding of the protein. Increased thermal fluctuations weaken the hydrogen bonds that maintain BSA's native helical structure, resulting in the disruption of cooperative hydrogen bonds and exposing hydrophobic regions to the solvent. This process facilitates aggregation via intermolecular hydrophobic and electrostatic interactions. Although BSA contains 34 disulfide-linked cysteine residues that could theoretically participate in the aggregation process, it is unlikely that these bonds were relevant in our case, as heat alone does not effectively break or reduce disulfide linkages. Initially, the solution was in a liquid state, transitioning to a jiggly gel, and ultimately forming a soft gel. Following this, the hydrogels were subjected to lyophilization at -80°C for 24 hours and subsequently stored at 4°C for further analysis. The synthesized hydrogels underwent comprehensive characterization to investigate various physical and chemical properties.

5.2.3 Characterizations of hydrogels

The scanning electron microscopy (SEM) images of the hydrogels (Fig 5.1D) reveal a porous architecture characterized by visible micron-sized voids. Notably, an increase in CNT concentration corresponds to a decrease in pore size, attributable to enhanced cross-linking within the hydrogel matrix. This observation underscores the capacity to modulate the hydrogel's structural properties by varying CNT concentrations, which in turn affects its physical characteristics. The morphological analysis further supports the notion of π–π stacking interactions between CNTs and the BSA-cellulose network within the hydrogel. As the concentration of CNTs rises, the hydrogel forms a more compact network structure with smaller pore sizes. This phenomenon can be explained by the high aspect ratio and surface area of CNTs, which provide additional interaction points and facilitate entanglement within

the BSA-cellulose framework. The resulting increased connectivity among polymer chains restricts the formation of larger pores, thereby enhancing the structural integrity and stability of the hydrogel. The variations in porosity among different composite hydrogel formulations are evident in the SEM images. For example, the formulation B+C+CNT3, which exhibits an elevated CNT concentration, shows a marked reduction in porosity, highlighting the tunability of the hydrogel's structural features based on CNT content.

The swelling behavior of CNT-based hydrogels was evaluated to determine their effectiveness as wound dressings (Fig 5.1E). Over a 24-hour period, the swelling ratio of the composite hydrogels increased with rising concentrations of CNTs (Fig. 5.1E). The control B and B+C hydrogels exhibited a swelling ratio of 350% and 400% respectively, while CNT-incorporated hydrogels showed significantly higher ratios, reaching up to 480%. This enhanced swelling is due not only to the hydrophilic nature of BSA but also to the unique properties of CNTs. CNTs contribute to the hydrogel's structure by improving the distribution of water within the matrix. Their high surface area facilitates the creation of additional crosslinking points, leading to a more uniform and interconnected pore structure that effectively traps water molecules.

Increased CNT concentrations promote better water absorption by reinforcing the hydrogel's network, while also maintaining its mechanical integrity. However, beyond a certain threshold, higher CNT levels may reduce pore size, limiting further swelling due to excessive crosslinking. As depicted in Fig. 5.1F, the degradation profile of the hydrogels over a 20-day period showed that CNT-based formulations-maintained stability with controlled weight loss. This combination of enhanced swelling and stability suggests that CNTs improve the hydrogel's ability to retain moisture, supporting prolonged wound coverage and providing an

optimal environment for healing. The ability of CNTs to balance water retention and structural integrity makes them a valuable addition to the hydrogel, enhancing its performance in wound healing applications.

The conductivity of CNT-based hydrogels plays a crucial role in facilitating wound healing by restoring the bioelectrical signal pathways that are typically disrupted at the wound site[164]. Conductive hydrogels can help reestablish these pathways, potentially accelerating the healing process[165]. By varying the concentration of CNTs within the hydrogel matrix, we were able to modulate both electrical (Fig 1G) and ionic conductivity (Fig 5.1H). The control BSA hydrogel (B) displayed a relatively low conductivity of 0.6378 S/m, while the addition of cellulose (B+C) slightly increased this value to 0.6993 S/m. However, the incorporation of CNTs led to a dramatic enhancement in conductivity. Specifically, B+C+CNT1 exhibited a conductivity of 4.4848 S/m, which increased to 6.7474 S/m for B+C+CNT2 and reached a maximum of 8.7734 S/m for B+C+CNT3. This increase is attributed to the unique conductive properties of CNTs, which form robust networks within the hydrogel, enabling more efficient charge transfer.

The improvement in conductivity is further supported by the hydrophilic nature of BSA and cellulose, which aids in water retention and boosts ionic conductivity. CNTs, with their high surface area, enhance water absorption and create additional crosslinking points in the matrix, leading to better ionic mobility. This combined effect of increased electrical and ionic conductivity is essential for maintaining a moist environment and promoting efficient cell communication at the wound site, thereby facilitating faster healing. The tunability of the hydrogel's conductivity through CNT concentration demonstrates the hydrogels' potential to mimic the natural conductive pathways of skin, making them promising candidates for

advanced wound healing applications. The balance between crosslinking density, water retention, and conductivity enables these hydrogels to support both structural integrity and optimal healing environments.

The rheological characterization of CNT-based hydrogels provides critical insights into their mechanical behaviour, particularly through amplitude and frequency sweep tests[129]. The amplitude sweeps (Fig 5.1I) analysis reveals key features such as yield stress and the linear viscoelastic range (LVR)[75]. In these hydrogels, a plateau region is observed in the storage modulus (G') at low strains, typically around 1%, indicating the presence of a stable, three-dimensional cross-linked network. The incorporation of carbon nanotubes (CNTs) enhances this plateau region, which contributes to increased structural stability and resilience against deformation. As strain increases, there is a gradual decrease in G', reflecting the material's ability to withstand applied stress while maintaining its integrity, which is essential for applications requiring injectable and smooth-textured hydrogels[86].

At low shear rates, the hydrogels predominantly exhibit elastic behavior, characterized by G' being greater than G''[166]. This indicates that the material can recover its shape after deformation, an essential property for applications involving dynamic environments[130]. However, as the shear rate increases, the hydrogels reach a point of dynamic yield stress where G' equals G'', transitioning to a more viscous behavior where G'' surpasses G'[14]. This behavior is indicative of the material's ability to flow under higher stress, making it suitable for injection-based applications[35].

Furthermore, frequency sweep (Fig 5.1J) tests conducted within the LVR highlight the predominantly elastic nature of the CNT-based hydrogels. Over a range of frequencies, G'

consistently exceeds G'', confirming the stability of the hydrogel network over time. Both G' and G'' remain nearly constant and independent across the frequency range, emphasizing the structural stability and elastic behaviour of the material[167]. This stability is vital for long-term storage and functionality in biomedical applications, ensuring that the hydrogels maintain their performance characteristics when subjected to varying mechanical conditions. Overall, the insights gained from these rheological tests underscore the potential of CNT-based hydrogels for tailored applications in clinical settings.

The mechanical properties of CNT-based hydrogels, particularly their compression and adhesion characteristics, are critical for their use in wound dressing applications[168]. Compression tests (Fig 5.1K) demonstrate that these hydrogels maintain excellent stability and structural integrity under stress, while their soft and stretchable nature suggests a high degree of cross-linking facilitated by the substantial water content in their porous structure. The addition of carbon nanotubes (CNTs) enhances the compression modulus, resulting in a resilient matrix capable of withstanding deformation while remaining flexible.

Adhesion plays a vital role in the early stages of wound healing, as the hydrogel must effectively bond to the wound site. Adhesive properties were evaluated through lap shear strength tests, where the hydrogel was applied to porcine tissue and allowed to set at a physiological temperature of 37 °C for several hours. The adhesive strength of the CNT-based hydrogels increased significantly with varying compositions (Fig 5.1L). The B hydrogel exhibited an adhesive strength of 1.5 ± 0.34 kPa, which rose to 3.3 ± 0.37 kPa for the B+C formulation. Further enhancements were observed with the inclusion of CNTs: B+C+CNT1 displayed an adhesive strength of 7.0 ± 0.87 kPa, B+C+CNT2 reached 9.44 ± 1.19 kPa, and B+C+CNT3 achieved 10.89 ± 1.14 kPa.

These findings illustrate that the incorporation of CNTs markedly improves the adhesive strength of the hydrogels, allowing them to form stronger bonds with biological tissues. This improvement in adhesion is likely due to the formation of intermolecular interactions, including hydrogen and ionic bonds, between the hydrogel and the tissue. Overall, the mechanical properties of CNT-based hydrogels, encompassing their compression behavior and adhesive capabilities, align well with the requirements for effective wound healing and tissue engineering. These characteristics highlight the potential of CNT-based hydrogels as effective materials for advanced wound dressings, where both mechanical stability and adhesive properties are essential for promoting healing and preventing complications.

5.2.4 Photothermal property, photothermal antibacterial and antioxidant activity

The photothermal properties of hydrogels enhanced with conductive components, such as carbon nanotubes (CNTs), are vital for their potential use in wound healing, particularly in addressing bacterial infections. These materials are characterized by their strong optical

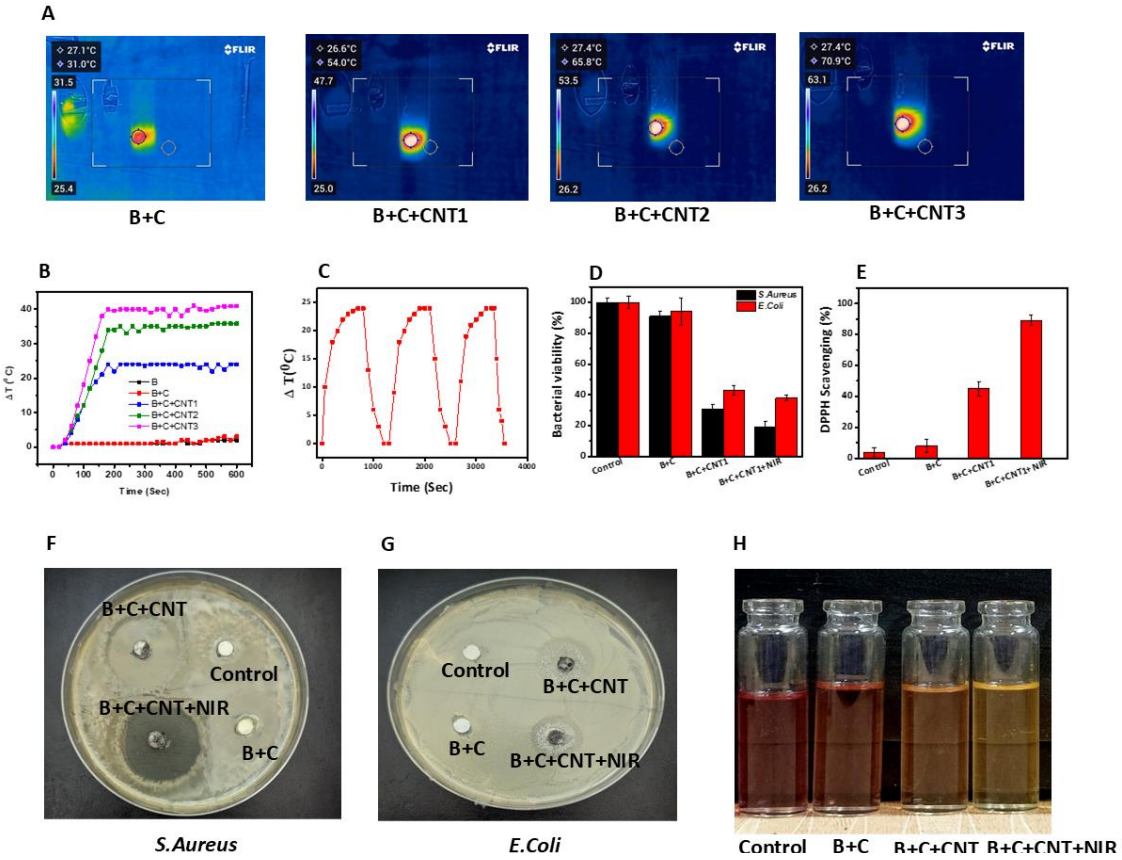

Figure 5.2 Thermal images of B+C+CNT hydrogels stimulated by NIR 808 nm irradiation for 5 min (B) Photothermal response of B+C+CNT hydrogels (C) Cyclic photostability of B+C+CNT1 hydrogel at 3 on/off cycles (D) NIR induced photothermal antibacterial effect of B+C+CNT hydrogels (E)NIR induced photothermal Antioxidant activity of B+C+CNT hydrogels (F,G) Pictorial representation of antibacterial activities (H) Pictorial representation of antioxidant activity via DPPH scavenging (Dats is represented as Mean± SEM (n=3))

absorption, which allows them to effectively convert near-infrared (NIR) light into heat as depicted in Fig 5.2A as thermal images of hydrogels captured by IR camera.

In the studied formulations, the temperature changes (ΔT) showed that both the B and B+C hydrogels had similar ΔT values of approximately 2 °C, indicating limited photothermal response (Fig 5.2B). In contrast, the introduction of CNTs significantly enhanced the photothermal behavior. The B+C+CNT1 formulation exhibited a ΔT of 28 °C, while B+C+CNT2 and B+C+CNT3 reached ΔT values of 38 °C and 43 °C, respectively. This increase underscores the strong correlation between CNT concentration and the hydrogels' ability to generate heat.

Furthermore, the stability of the photothermal response (Fig 5.2C) was evaluated by subjecting the B+C+CNT1 hydrogel to three cycles of NIR light exposure (5 minutes on, 5 minutes off). The experimental results indicated that this formulation maintained a consistent thermal profile throughout these cycles, demonstrating its robust photothermal stability. This stability is crucial for practical applications, as it ensures that the hydrogel can effectively respond to NIR irradiation over extended periods without significant degradation in performance[169].

Furthermore, we also evaluated effect of NIR based treatment of hydrogel with antibacterial (Fig 5.2D) and antioxidant assay (Fig 5.2E). The antibacterial assay results of the CNT-based hydrogels revealed a significant enhancement in bacterial inhibition for *S.aureus* (Fig 5.2F) and *E.coli* (Fig 5.2G) , particularly with the inclusion of CNTs and the use of near-infrared (NIR) irradiation. In the control group, bacterial growth was set at 100%, while the B+C

hydrogel without CNTs showed a slight reduction in bacterial growth, with 91% of bacteria remaining, indicating its limited antibacterial properties.

Upon incorporating CNTs, the B+C+CNT1 hydrogel demonstrated a dramatic reduction in bacterial growth, with only 31% of bacteria surviving. This improvement highlights the effective antibacterial nature of CNTs, likely due to their ability to disrupt bacterial cell membranes. Furthermore, the application of NIR irradiation to the B+C+CNT1 hydrogel (B+C+CNT1+NIR) resulted in even stronger antibacterial activity, reducing bacterial growth to 19%. This enhanced performance can be attributed to the photothermal effect of CNTs, where heat generated under NIR light may further damage bacterial cells and improve bacterial inhibition[170].

These results suggest that combining CNTs with NIR irradiation can significantly improve the antibacterial properties of hydrogels, making them highly effective in preventing infections in wound healing applications. The ability of the hydrogels to reduce bacterial growth so effectively underlines their potential as advanced materials for wound dressings, capable of providing both mechanical support and antibacterial protection.

The antioxidant activity of the hydrogels, evaluated through DPPH scavenging, demonstrated (Fig 5.2H) significant differences based on the formulation and exposure to NIR irradiation. The control sample showed minimal antioxidant activity with a DPPH scavenging rate of 4%. The B+C hydrogel exhibited a slight improvement with 8% scavenging, indicating limited antioxidant properties in the absence of CNTs. In contrast, the addition of CNTs dramatically enhanced the antioxidant capacity, with the B+C+CNT1 hydrogel showing a 45% scavenging effect. Notably, when exposed to NIR irradiation, the B+C+CNT1+NIR formulation

displayed an impressive 89% scavenging rate, underscoring the synergistic effect of CNTs and NIR light in boosting antioxidant performance. These results highlight the potential of CNT-based hydrogels, particularly under NIR light, to significantly reduce oxidative stress, which is essential for improving wound healing outcomes by protecting tissues from free radical damage.

5.2.5 In vitro studies

The biocompatibility of the hydrogels was assessed through cell viability (Fig 5.3A), hemolysis (Fig 5.3B), and FDA/PI staining assays (Fig 5.3C), highlighting their suitability for wound dressing applications. Cell viability was evaluated using the MTT assay on fibroblast cell lines (L929) after treatment with different hydrogel formulations over 24, 48, and 72 hours. The results demonstrated that the control group had a viability of 99.30 ± 1.18%, while the B+C, B+C+CNT1, and B+C+CNT1+NIR groups exhibited viabilities of 96.84 ± 1.85%, 98.73 ± 1.51%, and 100.51 ± 1.44%, respectively. These findings suggest that the hydrogels did not hinder cell growth, as evidenced by the increase in viable cells over time, with percentages exceeding 100% for the B+C+CNT1+NIR group at the 72-hour mark.

Hemolysis testing was conducted to evaluate the compatibility of the hydrogels with red blood cells (RBCs). The hemolysis percentages were minimal, with control at 100% hemolysis, B+C at 3.0 ± 0.12%, B+C+CNT1 at 4.0 ± 0.23%, and B+C+CNT1+NIR at 3.5 ± 0.34%. These results indicate that the hydrogels possess excellent hemocompatibility, showing negligible damage to RBC membranes, which is crucial for preventing adverse reactions in wound applications.

FDA/PI staining further corroborated the biocompatibility of the hydrogels. Fluorescent microscopy revealed a predominant green fluorescence in treated cells, indicating high viability and metabolic activity. The FDA staining confirmed that nearly all fibroblast and macrophage cells remained viable post-treatment, demonstrating that the hydrogels support cell health and proliferation. This qualitative analysis aligned with the quantitative viability data, reinforcing the potential of these hydrogels for promoting effective wound healing.

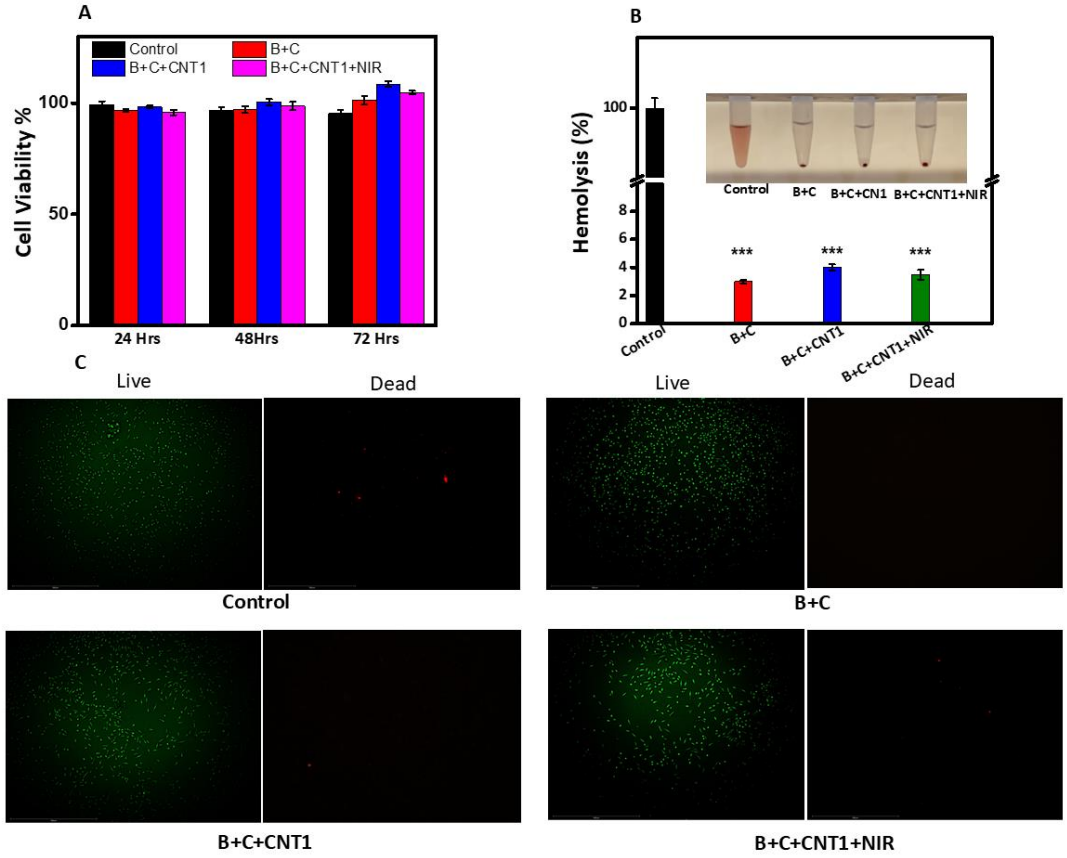

Figure 5.3 in vitro biocompatibility assessment of hydrogels (A) Cell viability of NIH 3T3 cell line (B) Hemolysis ratio of human blood cells (C) images of LIVE/DEAD staining of In summary, the collective data from cell viability, hemolysis, and FDA/PI assays indicate that the hydrogels exhibit strong biocompatibility, making them promising candidates for wound dressing applications.

5.2.6 In vivo study

The in vivo wound healing potential of the hydrogels was assessed in a diabetic mouse model, focusing on the effects of B+C, B+C+CNT1, and B+C+CNT1+NIR formulations on wound contraction over a period of 15 days. Excision wounds were created in streptozotocin (STZ)-induced diabetic rats, the hydrogels were applied locally, with some groups receiving NIR radiation to enhance therapeutic effects. Fig 5.4A represents pictorial representation of diabetic wounds on SD rats while Fig 5.4B represents thermal images of wounds with and without NIR groups.

At the observation period of 0^{th}, 4^{th} ,8^{th} and 14^{th} day, the wound areas were measured (Fig 5.4C). The control group exhibited a wound area of 101.23 ± 4.52 %. In contrast, the B+C group showed significant improvement with a wound area of 45 ± 3 %. The B+C+CNT1 group displayed further enhancement, with a reduced wound area of 19 ± 1.34 %. Remarkably, the group treated with B+C+CNT1+NIR achieved the minimal wound area of 4 ± 0.98 %, indicating superior healing. The faster healing observed in the B+C+CNT1+NIR group can be attributed to the dual properties of CNTs, which provide both enhanced electrical conductivity and photothermal effects. The increased electrical conductivity of the CNT-containing hydrogels facilitates cellular activities such as proliferation and migration, crucial for effective wound healing[171]. Furthermore, the photothermal properties of CNTs allow for localized heating upon NIR exposure, which can enhance blood flow and stimulate cellular responses that promote healing[172].

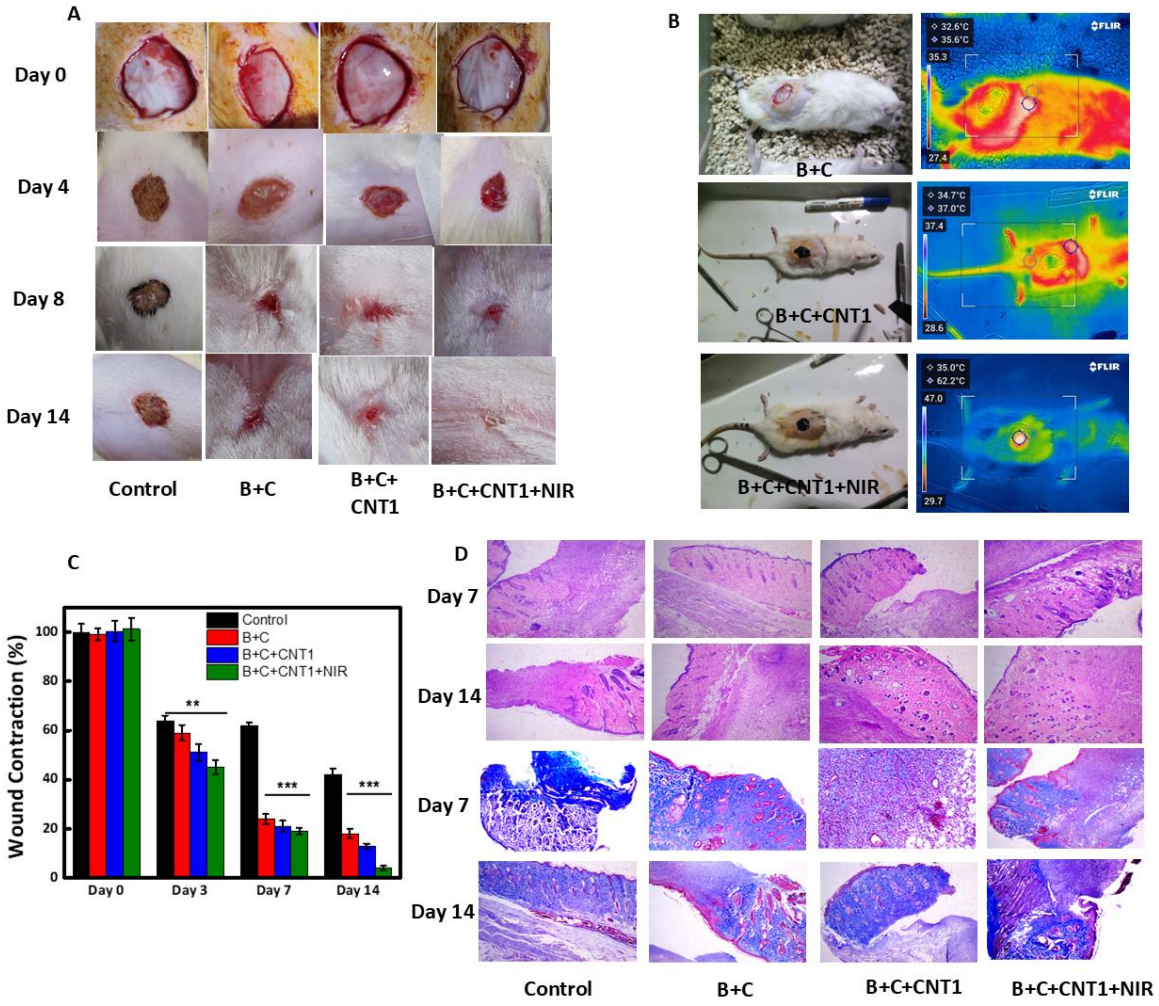

Figure 5.4 In vivo wound healing performance of B+C+CNT hydrogels with NIR treatment (A) Pictorial representation of wounds over 0th 4th 8th and 14th day (B) Infrared thermal images of rats wound irradiated with laser 808 nm (C) Percentage of wound closure rate (D) H&E and Masson's trichrome staining of wound tissues over 7 and 14 days

Histological evaluations were conducted using Hematoxylin and Eosin (H&E) staining to assess the overall tissue morphology and healing process in all groups as depicted in Fig 4D. The H&E staining indicated that the hydrogel-treated groups (B+C, B+C+CNT1, and B+C+CNT1+NIR) exhibited improved re-epithelialization and a well-organized structure compared to the control group, which showed signs of delayed healing. The dual properties

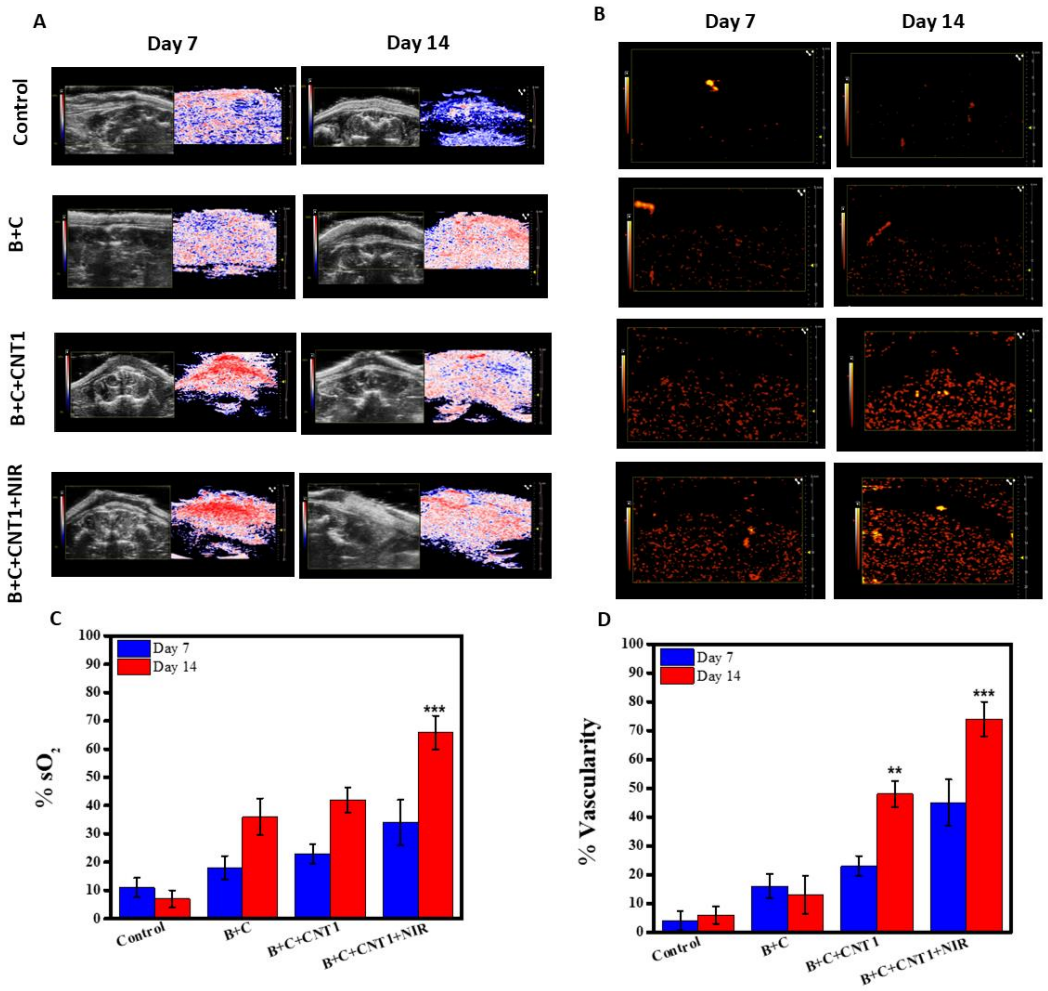

Figure 5.5 (A) ultrasound and photoacoustic imaging (B) Power doppler images of the wound over 7th and 14th days (C) %sO2 (D) % Vascularity of the wounds over 7th and 14th days (* $P < 0.05$, ** $P < 0.01$, *** $P < 0.001$)

of CNTs likely played a role in this improved tissue organization, influencing cellular behavior and supporting better tissue integration. Additionally, Masson's trichrome staining was performed to evaluate collagen deposition in the healed tissue across all groups. The staining results indicated that the control group had fewer collagen fibers, while the hydrogel-treated groups demonstrated denser, thicker, and more uniform collagen fibers. Notably, the B+C+CNT1+NIR group exhibited the most uniform and dense collagen deposition,

suggesting enhanced tissue regeneration. The conductivity of the hydrogels may facilitate collagen synthesis and organization, while the photothermal effect can further stimulate fibroblast activity and collagen production.

These results indicate that the incorporation of CNTs and the application of NIR radiation significantly enhance the wound healing process. The dual properties of conductivity and photothermal effects in the B+C+CNT1+NIR group support superior tissue regeneration and healing capability.

5.2.7 Real time tracking via Photoacoustic imaging

The therapeutic efficacy of the hydrogels was further evaluated using photoacoustic imaging Fig 5.5A) and power Doppler techniques (Fig 5.5B), which provide insights into blood flow, oxygenation levels and vascularization during the wound healing process[173].

On day 7, the percentage of oxygenated blood showed notable differences across the treatment groups (Fig 5.5C). The control group exhibited an oxygenation level of 11% ± 3.5, while the B+C group improved this to 18% ± 4.2. The B+C+CNT1 group achieved 23% ± 3.45, reflecting a significant enhancement in oxygenation. Most impressively, the B+C+CNT1+NIR group demonstrated an oxygen saturation level of 34% ± 8, indicating the substantial impact of NIR radiation in promoting blood oxygen levels. On day 14, the results further highlighted the effectiveness of the treatments. The control group demonstrated an oxygenation level of 7% ± 3, while the B+C group showed a substantial increase to 36% ± 6.5. The B+C+CNT1 group improved oxygenation to 42% ± 4.5, and the B+C+CNT1+NIR group reached 65.8% ± 6, reflecting a marked enhancement in oxygen delivery to the wound site. Similarly, vascularity measurements obtained through power Doppler imaging provided

further insights into the healing process (Fig 5D). On day 7, the control group had a vascularity percentage of 4% ± 3.5. The B+C formulation increased vascularity to 16% ± 4.2, while the B+C+CNT1 group showed improved vascularity at 23% ± 3.45. Again, the B+C+CNT1+NIR group exhibited the highest vascularity at 45% ± 8, underscoring the significant enhancement in blood flow to the healing tissue, especially with the added benefit of NIR treatment. In terms of vascularity on day 14, the control group showed a percentage of 6% ± 3. The B+C group improved this to 13% ± 6.5, while the B+C+CNT1 group demonstrated a significant vascularity increase to 48% ± 4.5. The B+C+CNT1+NIR group again led with a vascularity percentage of 74% ± 6, emphasizing the crucial role of both CNTs and NIR treatment in enhancing blood flow to the healing tissue.

Overall, the photoacoustic and power Doppler imaging studies confirm that the application of B+C+CNT1 and B+C+CNT1+NIR hydrogels leads to significantly enhanced healing rates, driven by increased vascularity and oxygenation. This approach holds promise for developing advanced wound care treatments that can effectively address chronic wounds and improve patient outcomes.

5.2.8 Immunohistochemistry

In the immunohistochemistry (IHC) analysis of wound healing, we explored the expression of inflammatory markers and angiogenesis markers through CD68 (Fig 5.6A-B), α-SMA (Fig 5.6C-D), and CD31 (Fig 5.6E-F) staining at days 7 and 14, which provides insights into inflammation resolution and vascular regeneration during the healing process of the hydrogels. On day 7, the wound sections stained for CD68—a marker for macrophages—revealed a significant accumulation of inflammatory cells in the control and B+C groups.

These groups exhibited dense brown staining, indicating persistent inflammation. In contrast, the B+C+CNT1 and especially the B+C+CNT1+NIR groups showed a marked reduction in CD68-positive cells, suggesting a decrease in macrophage infiltration and a faster resolution of inflammation in these groups[174]. By day 14, there was a further reduction in CD68-positive staining in the B+C+CNT1+NIR group, showing that the dual properties of carbon nanotubes (CNTs)—conductivity and photothermal effect—help modulate inflammation more effectively than other groups. The expression of α-SMA (alpha-smooth muscle actin), a marker for myofibroblast activity associated with wound contraction, was also examined[175]. On day 7, the control and B+C groups showed limited α-SMA staining, reflecting less myofibroblast activity and slower wound contraction. However, the B+C+CNT1 and B+C+CNT1+NIR groups had more intense α-SMA staining, indicating enhanced myofibroblast activity. This suggests that CNTs, particularly under NIR treatment, can stimulate more robust wound contraction due to the material's conductivity, promoting rapid wound closure. By day 14, α-SMA staining was even stronger in the B+C+CNT1+NIR group, confirming that the combined conductivity and photothermal properties of the CNTs led to accelerated wound contraction and tissue remodelling. To evaluate new blood vessel formation, we performed staining for CD31, a marker for endothelial cells involved in angiogenesis. On day 7, minimal CD31 staining was observed in the control and B+C groups, indicating poor vascularization. However, the B+C+CNT1 and B+C+CNT1+NIR groups exhibited significantly higher CD31 expression, reflecting increased angiogenesis. Notably, the B+C+CNT1+NIR group showed the most prominent CD31-positive staining, suggesting that the combination of CNT and NIR treatment not only promotes vascularization but also enhances oxygen and nutrient supply to the wound site[176]. By day 14, this trend continued,

with the B+C+CNT1+NIR group demonstrating the highest level of vascularization, facilitating faster tissue repair and regeneration. The immunohistochemical findings for CD68, α-SMA, and CD31 demonstrate that the B+C+CNT1+NIR group showed the most promising results in reducing inflammation, promoting wound contraction, and enhancing vascularization. This suggests that the combination of carbon nanotubes with NIR treatment provides a dual advantage: the conductivity of CNTs facilitates faster cell signalling and wound closure, while the photothermal effect under NIR enhances antibacterial properties and tissue regeneration.

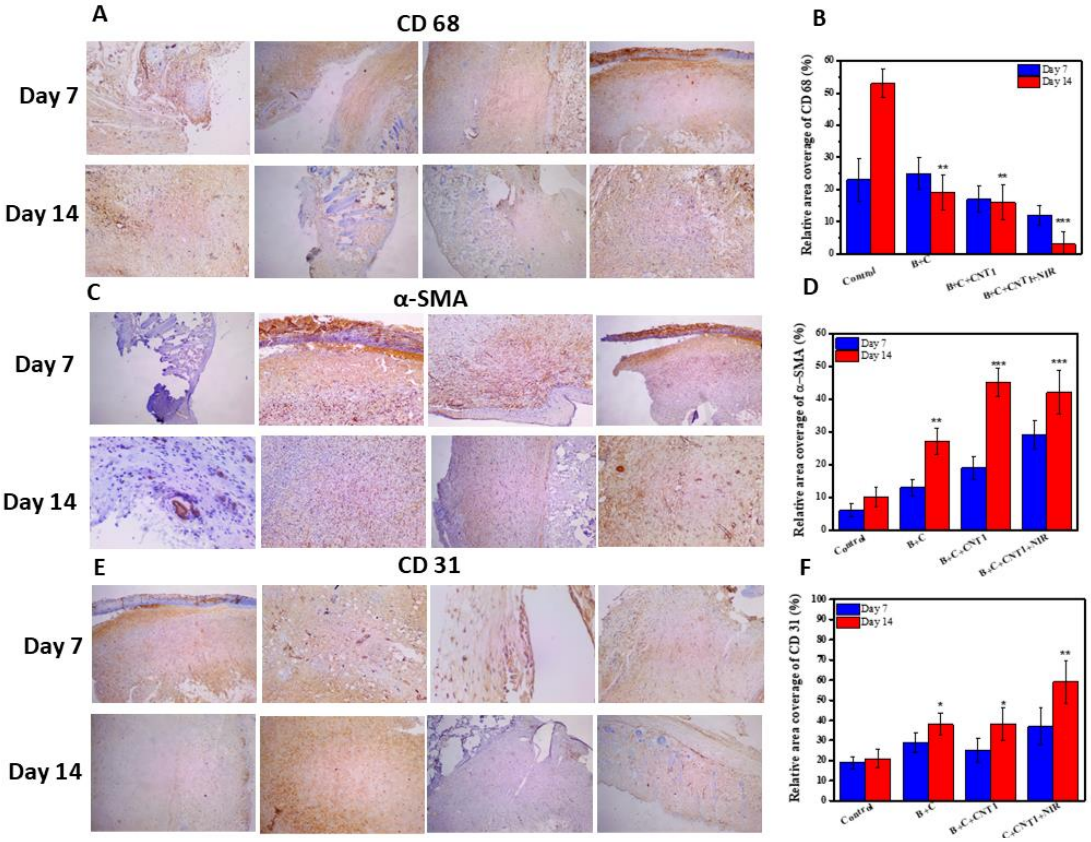

Figure 5.6 Immunohistochemical staining of skin wounds 7th and 14th days (A) pictorial representation and (B) qualitative analysis of CD 68 (C) pictorial representation and (D) qualitative analysis α-SMA (E) pictorial representation and (F) qualitative analysis of CD 31

5.3 Conclusion

This study demonstrates the efficacy of a novel carbon nanotube (CNT)-based conductive protein-cellulose hydrogel in promoting diabetic wound healing through photothermal therapy. The hydrogel exhibited excellent biocompatibility, enhanced conductivity, and controlled biodegradability, making it a suitable candidate for wound treatment. In vivo experiments on diabetic wounds showed accelerated healing in the CNT-loaded hydrogels, particularly when combined with near-infrared (NIR) irradiation, attributed to the dual properties of CNTs—conductivity and photothermal effects. This combination significantly reduced inflammation, enhanced collagen deposition, and promoted angiogenesis, as confirmed through histological analysis, immunohistochemistry for CD68, α-SMA, and CD31 markers, and wound contraction measurements. Moreover, the integration of photoacoustic imaging provided non-invasive real-time tracking of wound healing, illustrating enhanced vascularity and oxygenation in the NIR-treated groups. Overall, the CNT-based hydrogel, especially when combined with NIR, holds great promise as a multifunctional wound dressing for treating chronic diabetic wounds, offering both therapeutic and diagnostic capabilities.